Published in final edited form as:
J Magn Reson Imaging. 2013 October ; 38(4): 885–896. doi:10.1002/jmri.24053.

Comparison of Brown and White Adipose Tissues in Infants and Children with Chemical-Shift-Encoded Water-Fat MRI

Houchun H. Hu, PhD[1], **Larry Yin, MD, MSPH**[2], **Patricia C. Aggabao, BA**[1], **Thomas G. Perkins, PhD**[3], **Jonathan M. Chia, MS**[3], and **Vicente Gilsanz, MD, PhD**[1]
[1]Department of Radiology, Children's Hospital Los Angeles, Los Angeles, California, USA

[2]Department of Pediatrics, Children's Hospital Los Angeles, Los Angeles, California, USA

[3]Philips Healthcare, Cleveland, Ohio, USA

Abstract

Purpose—To compare fat-signal fractions (FFs) and T_2* values between brown (BAT) and white (WAT) adipose tissue located within the supraclavicular fossa and subcutaneous depots, respectively.

Materials and Methods—Twelve infants and 39 children were studied. Children were divided into lean and overweight/obese sub-groups. Chemical-shift-encoded water-fat MRI was used to quantify FFs and T_2* metrics in the supraclavicular and adjacent subcutaneous adipose tissue depots. Linear regression and t-tests were performed.

Results—Infants had lower supraclavicular FFs than children ($p<0.01$) but T_2* values were similar ($p=0.5$). Lean children exhibited lower supraclavicular FFs and T_2* values than overweight children ($p<0.01$). In each individual infant and child, supraclavicular FFs were consistently lower than adjacent subcutaneous FFs. Supraclavicular T_2* values were consistently lower than subcutaneous T_2* values in children, but not in infants. FFs in both depots were positively correlated with age and weight in infants ($p<0.01$). In children, they were correlated with weight and BMI ($p<0.01$), but not age. Correlations between T_2* and anthropometric variables existed in children ($p<0.01$), but were absent in infants.

Conclusion—Cross-sectional comparisons suggest variations in FF and T_2* values in the supraclavicular and subcutaneous depots of infants and children, which are potentially indicative of physiological differences in adipose tissue fat content, amount, and metabolic activity.

Keywords

Brown adipose tissue; white adipose tissue; water-fat MRI; fat-signal fraction; T_2* relaxation; children

INTRODUCTION

There has been a resurgence of interest in brown adipose tissue (BAT) over the past few years (1). The plethora of recent findings of human BAT with positron emission and computed tomography (PET/CT) imaging has reinvigorated research focus in the tissue's role in obesity and metabolic diseases (2). Numerous PET/CT studies in adults have

Corresponding Author: Houchun H. Hu, PhD Children's Hospital Los Angeles 4650 Sunset Boulevard, Department of Radiology, MS #81 Los Angeles, California, USA. 90027 hhu@chla.usc.edu, houchunh@usc.edu office: +1 (323) 361-2688 fax: +1 (323) 361-1510 .

demonstrated an inverse association between body adiposity and the presence of metabolically active, or functional, BAT (3-6). Overweight subjects with high body-mass-indices (BMI) typically do not exhibit BAT uptake of 18F-FDG radiotracer in comparison to leaner subjects (7, 8). Although BAT was traditionally believed to be present in all neonates and thought to be gradually lost after infancy, recent works have demonstrated on the contrary that metabolically active BAT is prevalent in pediatric and adolescent cohorts (9-11), as well as in adults (12, 13).

In contrast to white adipose tissue (WAT), which stores triglycerides, BAT metabolizes fat to generate heat. While WAT is characterized by large adipocytes that contain a single intracellular triglyceride droplet and is sparsely perfused by blood, BAT typically contains smaller adipocytes with multiple intracellular triglyceride droplets. BAT also contains significant intracellular water, is replete with iron-rich mitochondria, and is densely vascularized by capillaries. Whereas the detection of BAT by PET/CT is highly dependent on tissue function and radiotracer uptake (6), the intrinsic morphological differences between BAT and WAT can give rise to unique signals that can be alternatively detected by magnetic resonance imaging (MRI). Several recent works have exploited these concepts and demonstrated the feasibility of BAT MRI in mice, and have identified distinct BAT properties including zero-quantum spectral interactions (14), fat-signal fractions (FFs) (15), and T_2 and T_2* relaxation times in relation to blood perfusion (16, 17), in contrast to triglyceride-rich WAT. Collectively, these studies support quantitative MRI as a platform capable of characterizing BAT in humans. Since MRI does not involve ionizing radiation and does not necessarily require an exogenous radiotracer, it can be more broadly utilized in asymptomatic and healthy cohorts, including infants and children.

The underlying premise for variations in FF and T_2* values in BAT has been described in previous reports and both MRI biomarkers have been shown in mouse studies to be related to the animal's interscapular BAT, the former reflecting the relative amount of triglycerides present within the tissue (15, 18), and the latter suggestive of the level of intracellular iron and blood oxygenation and perfusion to the tissue (16, 17). Thus with greater metabolic activity, BAT becomes characterized by lower FF values due to a combination of increasing oxidative metabolism of intracellular fat stores and enhanced tissue blood flow, while lower T_2* values can be attributed to increasing oxygen consumption and rising deoxyhemoglobin levels in the local circulating blood (19-21).

Building on prior MRI works and recent case reports (22), we extend the current investigation to infants and children. Based on findings that BAT FF and T_2* differences manifest between lean and obese mice (18), with both parameters significantly lower in the lean, the primary purpose of this work was to determine whether such trends can be observed cross-sectionally in the supraclavicular fossa BAT depot in lean ($<85^{th}$ percentile BMI) and overweight ($\geq 85^{th}$ percentile BMI) children of similar age. We hypothesize that BAT FF and T_2* measurements will be similarly lower in lean children than their overweight counterparts. A second goal of the study was to compare the two MRI metrics between infants under six-months of age and children. Additionally, a third goal of the study was to obtain FF and T_2* values of subcutaneous WAT and compare them against corresponding BAT measurements. Lastly, the study aimed to determine correlations between these MRI measurements, subject age, and anthropometric variables of weight and BMI.

MATERIALS AND METHODS

Study Cohort

Local institutional review board approvals were obtained for this study and all participants and/or their legal guardians gave assent/consent. The top portions of Table 1 and Table 2 summarize demographic and anthropometric variables for the infant (n=12, 5 boys, 7 girls) and children cohorts (n=39, 31 boys, 8 girls), respectively. Note that age for the infants is reported in days. Weight percentiles for were computed according to appropriate World Health Organization growth charts. BMI percentiles were computed for children based on Centers for Disease Control and Prevention guidelines. In Table 2, distributions are given for all children as a group and also for two sub-groups, based on a BMI stratification at the standard 85^{th} percentile. Note that the two sub-groups (lean, n=17, 12 boys, 5 girls; overweight/obese, n=22, 19 boys, 3 girls) have similar ages. In the overweight/obese sub-group, four subjects, all boys, were considered overweight (between 85^{th} and 95^{th} BMI percentiles), while the remainder were considered obese (greater than 95^{th} BMI percentile). In the lean sub-group, only one subject, a female, was considered underweight with a BMI percentile of 4%, while all others were categorized with normal healthy BMIs. The infants were patients at our institution who were receiving routine neural MRI examinations as part of their medical care. Lean children were recruited as volunteers from the general population. Overweight and obese children were referred from our institution's outpatient obesity clinic by their pediatrician. Both infants and children were predominantly of Hispanic and Caucasian backgrounds. For the infants, no exclusion criteria were chosen, as long as informed consent was obtained. For the children, age and BMI were the only two criteria for determining eligibility.

Water-Fat MRI

All MRI exams were performed on a 3 Tesla human platform (Achieva, R3.2, Philips Healthcare, Cleveland, Ohio), at a room (MRI suite) temperature of approximately 25° Celsius. No contrast agents were administered nor were any of the participants subjected to additional cold temperature preparations (5-7) or pharmacological agents to purposely stimulate or suppress BAT activity. The multi-echo mDIXON chemical-shift water-fat multi-echo pulse sequence provided by the manufacturer was utilized in this work (23). Typical imaging parameters and setup for the 3D Cartesian spoiled-gradient-echo sequence were: supine, coronal or axial acquisition, TR=13-16 msec, first TE=1.2–1.4 msec, echo spacing=1.1–1.2 msec, number of TEs=6, non-flyback (bipolar) readout gradients, 75–175 2-mm overlapping slices reconstructed to 1 mm, flip angle=3°, bandwidth=1.3 kHz/pixel, SENSE acceleration=2, no respiratory or cardiac gating, and number of signals averaged=1. Average scan time for the mDIXON sequence was 5-7 minutes in children and 2-3 minutes in infants. Volume coverage was prescribed to adequately cover the full extent of the anatomy in the anterior/posterior and right/left directions at the level of the shoulder. The scan times differed largely because the voxel resolution was kept the same across all exams between infants and children. Thus, depending primarily on field-of-view (FOV) settings, the acquisition matrix (e.g. number of readout samples and phase encoding views) and the number of slices varied, thus leading to generally longer scan times in children, especially for those in the overweight/obese sub-group. Typical right/left FOV for the infants was 22-30 cm; for lean children, it was set to 34-40 cm; and for overweight/obese children, a 44-48 cm right/left FOV was prescribed. An 8-channel head coil was used in the infants and a 16-channel torso array was used in the children. Both coil arrays are commercially available from Philips Healthcare. Following our institution's pediatric Radiology protocol for routine neural MRI, none of the infants reported in this study were sedated with anesthesia. They were bottle-fed prior to being swaddled snuggly with blankets and placed in the MRI scanner. All children in this study were also not sedated and were awake during

their MRI exams. The use of anesthesia has been previously shown to influence BAT activity (24).

The mDIXON technique employed in this work is a six-echo generalization of the traditional in/opposed phase two-echo Dixon water-fat imaging technique. Image reconstructions yield co-registered water, fat, in-phase, and opposed-phase image series, and quantitative FF and T_2* maps after data acquisition, similar to the IDEAL method (25). The FF maps can accurately reflect the underlying proton density ratios between fat and the sum of water and fat on a range of 0-100% when a multi-peak spectral model of fat and a small excitation flip angle (26) are used. In this work, a seven-peak fat model was adopted (27). The multi-echo water-fat algorithms can jointly estimate FF and T_2* on a voxel-wise basis, with the latter metric being considered a factor that needs to be accounted for in order to facilitate accurate computation of the former. Both FF and T_2* metrics have been used in assessing hepatic fat and iron-overload (28-30). In the infants, the mDIXON sequence was the only research pulse sequence performed in addition to our institution's standard neural MRI protocols. In the children cohort, the mDIXON scan was the only pulse sequence implemented, aside from the requisite three-plane localizer and coil calibration scans.

Data Analysis

Image analysis was performed with sliceOmatic® (Version 5.0, Tomovision, Inc., Magog, Canada) segmentation software to compute mean and standard deviation FF and T_2* values from the bilateral adipose tissue depots (presumably BAT) within the supraclavicular fossa as well as the adjacent subcutaneous adipose tissue (presumably WAT) depot. For brevity, these two locations will heretofore be referred to simply as the supraclavicular fossa and subcutaneous depots and the phrase adipose tissue will be omitted. An experienced operator familiar with the software in conjunction with guidance from a pediatric radiologist performed the image segmentations. Care was taken during segmentation to exclude major blood vessels, bone and bone marrow (scapula, clavicle), and nearby muscles (trapezius, sternocleidomastoid). We chose to focus on the supraclavicular fossa depot because it is a large fat pad that is easily identifiable on anatomical images and has been extensively described in PET/CT literature of BAT (31). Specifically, the anterior deep fat pad, bound by the trapezius muscle posteriorly, the sternocleidomastoid muscle medially, and the clavicle inferiorly, was outlined. On the same imaging slices, the adjacent subcutaneous depot was similarly outlined. Figure 1 illustrates the manual analysis process and how segmentation masks were generated with sliceOmatic® software in an infant example. Reconstructed water, fat, and opposed-phase image series from the mDIXON sequence were used to provide anatomical guidance. Regions-of-interest (ROI) were drawn directly on these co-registered grayscale images first. The sliceOmatic® software subsequently transferred the ROIs automatically to the co-registered FF and T_2* maps for quantification. The signal-intensity-based 'Region Growing' and the 'Morphology' erosion tools were used to manipulate the ROIs on the grayscale water, fat, and opposed-phase images such that non-adipose tissue structures and partial volume voxels at adjacent tissue boundaries were avoided. Figure 2 additionally illustrates coronal examples of the adipose tissue depot segmentation process in children.

Based on extensive prior literature results in mice (14-18) and humans (22, 31), we assume that measurements of FF and T_2* in the human supraclavicular fossa depot are reflective of the relative tissue density and amount of BAT within this fat pad. If the supraclavicular fossa fat pad consists mostly of triglyceride-rich WAT adipocytes and is nearly devoid of BAT, higher FF and T_2* values would be expected. Conversely, if the supraclavicular fat pad is abundant with BAT adipocytes, lower FF and T_2* values would generally be expected. The size and amount of intracellular fat droplets in brown adipocytes can vary depending on the tissue's underlying level of stimulation and state of activity (32), thus

leading to potentially a large range of FF values reflecting small, fat-depleted droplets at one extreme, to enlarged, triglyceride-rich droplets at the other. Regardless of the size of fat droplets, the T_2* of BAT should remain lower than that of WAT, due to the presence of iron-laden mitochondria within brown adipocytes and BAT's greater blood perfusion. The *t*-test and linear regression (Statview v5.0.1; SAS Institute Inc., Cary, North Carolina) were used to assess the data, using a criterion of $p<0.05$ to conclude statistical significance.

RESULTS

Figure 3 illustrates representative images from two infants (A-D). FF and T_2* maps are shown in the left and right columns, respectively. Matching arrows and arrowheads highlight the bilateral supraclavicular fossa BAT and the subcutaneous WAT depots. The supraclavicular fossa depot appears uniquely in shades of blue, green, and yellow (~30-70% FF), distinct from the appearance of the triglyceride-rich subcutaneous depot (red) and lean skeletal muscles and water-dominant organs (purple). The two infants had identical body weights (~5.5 kg) at the time of their MRI exams. However, the infant shown in Figure 3 (A, B) had a weight percentile of 10%, versus 25% weight percentile for the infant shown in Figure 3 (C, D). Their mean supraclavicular fossa FFs were significantly different (38.5% vs. 53.7% vs.), respectively. The leaner infant also had a slightly lower mean T_2* value in the supraclavicular fossa depot (15.0 msec vs. 18.4 msec). The two infants also exhibited very similar FF measurements from the subcutaneous depot (85.9% vs. 86.8%), and T_2* values were again slightly lower in the leaner infant (24.3 msec vs. 27.2 msec). The lower FF and T_2* values of the supraclavicular fossa depot in comparison to the subcutaneous depot are in agreement with previous findings in mice (18).

Representative results from two children are similarly shown in Figure 3 (E-H). It is visually evident that the subject illustrated in Figure 3 (E, F) is lean, while the subject shown in Figure 3 (G, H) is obese. Note the near absence of subcutaneous adipose tissue in the lean child, especially along the axilla, in contrast to the obese case. In the latter, note that the highlighted supraclavicular fossa depots appear very WAT-like and are nearly indistinguishable from the adjacent subcutaneous depot on both FF and T_2* maps. For the lean child, supraclavicular fossa FF and T_2* measurements were 68.7% and 15.9 msec, respectively. For the obese child, they were both higher, at 85.4% and 23.6 msec, respectively. In the subcutaneous depot, FF and T_2* measurements for the lean child were 85.1% and 26.2 msec, respectively, in comparison to higher values of 91.2% and 34.6 msec for the obese child.

Table 3 summarizes linear regression coefficients between age, anthropometric variables, and MRI FF and T_2* measurements for both infants and children. Note that statistically significant correlations ($p<0.01$) were observed between FF and T_2* measurements versus weight, weight percentile, BMI, and BMI percentile in children from both the supraclavicular fossa and subcutaneous depots. In infants, correlations were the strongest with age and weight.

Figure 4 (A, B), accompanied by the bottom portions of Table 1 and Table 2, provide a summary of MRI measurements comparing the infant cohort versus the children cohort. The infant group was characterized by significantly lower FFs in the supraclavicular fossa depot (38.2±11.5%) than children (72.9±12.1%), although T_2* values between the two groups were comparable and not statistically different (18.8±4.8 vs. 18.0±3.6 msec). The infant group was also characterized by lower FFs in the subcutaneous depot (77.9±9.1%) than children (86.2±6.5%), and corresponding T_2* values were likewise lower in infants than in children (21.0±4.8 vs. 27.2±6.8 msec). Note that in both groups, FF and T_2* distributions were consistently lower in the supraclavicular fossa depot than in the corresponding

subcutaneous depot of the same group, albeit not statistically significant for T_2* in infants. As shown in Figure 4 (C, D), statistically significant linear correlations were found between FF measurements from both depots versus age and weight in the infant group, suggesting the possibility of rapid triglyceride accumulation within intracellular vacuoles in both brown (supraclavicular) and white (subcutaneous) adipocytes at these locations during this early stage of life. As further summarized in Table 3, T_2* measurements in the supraclavicular fossa depot however did not correlate with age or any anthropometric variables in the infant group, while T_2* measurements in the subcutaneous depot only moderately correlated with weight, but not age.

Figure 5 (A, B), in conjunction with Table 2, further compares differences in FF and T_2* measurements between the two lean and overweight/obese children sub-groups, stratified at the 85th BMI percentile. It is evident that lean subjects were characterized consistently by lower FF and T_2* values than their overweight/obese counterparts in both the supraclavicular fossa and subcutaneous depots. As shown in Figure 5 (C, D), statistically significant linear correlations were found between FF and T_2* distributions from both depots and BMI (and likewise weight) when considering all 39 children data points. As further summarized in Table 3, in contrast to findings from the infants, interestingly no statistically significant correlations between MRI measurements and age were observed. The apparent strong associations of both MRI biomarkers with body adiposity and the lack of such associations with age are supportive of past literature reports describing the rapid increase in white, and not brown, adipocyte cell size and number during this pubertal and adolescent growth stage of life (33, 34). For both FF and T_2* measurements from the supraclavicular fossa depot, none of the correlations with BMI and weight were statistically significant when considering only the lean sub-group. They were however statistically significant when considering only the overweight/obese sub-group. For both FF and T_2* measurements from the subcutaneous depot, no statistically significant correlations were observed with age or any anthropometric variable in both lean and overweight/obese sub-groups.

Figure 6 (A, B) illustrates two scatter plots of individual mean FF and T_2* measurements in infants and children, respectively. This pair of plots complements the findings in Figure 4 and Figure 5. First, it further emphasizes the absence of T_2* differences between supraclavicular fossa and subcutaneous adipose tissue in infants. Second, in children, it highlights the parallel increase in FF and T_2* values in both depots with progressively greater body adiposity. The latter data trend is visually striking and supports the notion that with increasing body adiposity (e.g. BMI percentile), both supraclavicular and subcutaneous depots become overridden with white adipocytes, thereby independently elevating the tissue's FF and T_2* values. It should be noted that the purpose of the scatter plots is not to imply a direct correlation between FF and T_2* measurements. Rather, FF and T_2* metrics are proposed as two separate measures of adipose tissue characteristics.

Figure 7 shows exemplary coronal FF maps from a 6-days-old female infant. This infant's data points are highlighted by arrows in Figure 6 (A). Note the rather low FF appearance of the subcutaneous adipose tissue depot in comparison to the older infants illustrated in Figure 3. Considering the trend shown in Figure 4 (C) between FF and age, it is speculated that the subcutaneous adipose tissue depot in newborns is abundant with brown adipocytes (35), and that with postnatal development, the depot becomes predominantly occupied by white adipocytes (36). In Figure 7 (B), the unique appearance of tissue at the nape suggestive of BAT is highlighted (31, 37).

DISCUSSION

In this cross-sectional study, we have extended the application of water-fat MRI to quantitatively measure differences in FF values and T_2* relaxation times within the supraclavicular fossa and subcutaneous depots between infants and lean and overweight/obese children. Our findings support this pair of metrics as complementary MRI biomarkers and as one strategy to characterize brown and white adipose tissue within these two depots. The lower proportion of intracellular triglycerides and greater proportion of mitochondria in brown adipocytes, coupled with a higher degree of blood perfusion and deoxyhemoglobin during stimulated metabolic activity, contributes to the overall reduction in FF and T_2* values of the tissue in comparison to triglyceride-rich WAT. The statistically significant positive correlations exhibited between supraclavicular fossa FF and T_2* values versus BMI, weight, and corresponding percentiles in the present children data, along with the scatter plot in Figure 6 (B), reinforce published PET/CT reports in adults that BAT is inversely related to body adiposity, and further underscore the additional efforts needed to elucidate the role of BAT in human physiology, metabolism, and obesity, and the tissue's potential clinical relevance.

It should be recognized at this point that the current cross-sectional work has only acquired MRI data and measured signal attributes of the two adipose tissue depots at a single time point. In the context of this study, the reported measurements characterize the underlying morphology of the tissue, not its metabolic activity. One should note that the current measurements of FF and T_2* are not a direct reflection of absolute BAT mass or volume within the supraclavicular fossa and subcutaneous depots, but rather a signal-based characterization of the depot that is suggestive of the potential presence of BAT and WAT. One necessary direction of future work is to develop a protocol to characterize FF and T_2* dynamically, ideally in a single MRI session before, during, and after a paradigm that is known to stimulate BAT, either with a pharmacological agent dose (16, 17) or by acute cold temperature exposure (5-7). Another attractive direction of future work is to monitor longitudinally FF and T_2* signal characteristics of the two adipose tissue depots individually from birth. It is perhaps this application that the approach to scatter plot FF and T_2* values, as demonstrated in Figure 6, can find potential value in elucidating human BAT physiology. Similarly, longitudinal intra-subject monitoring of FF and T_2* values in response to intervention (e.g. weight loss), coupled with additional measures such as energy expenditure (e.g. calorimetry), are needed to determine the metabolic capacity of BAT in humans.

In the context of the present MRI data, we speculate that BAT located within the supraclavicular fossa depot was metabolically active in all of the infants and in the sub-group of lean children. In contrast, we suspect that BAT was non-functional in the sub-group of overweight and obese children, consequently resulting in their WAT-like imaging appearance. These speculations support the notion that if unstimulated, prolonged inactivity of BAT can lead to an accumulation of triglyceride stores and an enlargement of intracellular triglyceride vacuoles, thereby causing the tissue to mimic a WAT phenotype. Indeed, it has been demonstrated that intracellular triglyceride droplets and mitochondria organelles within brown adipocytes can vary in size and number, depending on the tissue's underlying level of stimulation and activity (32).

Alternatively, it is also plausible that the density of BAT within the supraclavicular fossa depot of overweight and obese subjects is low and "invisible" to the mDIXON imaging method and the spatial resolution employed in this work. While prior autopsy results from post-mortem cases in infants suggest (22) that their supraclavicular fossa depots are quite abundant in the amount of BAT adipocytes, in adults, it has been shown that small clusters of a few brown adipocytes can be surrounded by an overwhelming number of larger white

adipocytes in the supraclavicular fossa depot (13), leading to a scenario that can likely create partial-volume effects and one that extends beyond the detection sensitivity of current water-fat MRI protocols. Thus, the accurate identification and characterization of BAT in overweight subjects have greater likelihood of being susceptible to partial-volume effects.

Another explanation that can be supported by the present imaging results is that the supraclavicular depots in the overweight subjects were completely devoid of BAT. In other words, BAT was absent. Although logical, this thought is contradictory to the current paradigm that BAT persists throughout life and does not disappear after birth. The aforementioned suggestion to longitudinally collect FF and T_2* measurements from birth to adulthood would be highly relevant in this regard. Complementary intermolecular zero-quantum coherence spectroscopy techniques that are insensitive to partial-volume effects and can unambiguously detect the presence of BAT with unique BAT-specific signals and relative independence to spatial resolution (14) would have been useful to further resolve and characterize BAT and possibly strengthen the outcome of this work. However, the feasibility of such techniques at clinical magnetic field strengths of 1.5 and 3.0 Tesla has not yet been demonstrated in humans. This demonstration or the demonstration of another comparable method is critical, as it is important to recognize that the present FF and T_2* metrics from water-fat MRI are not unique measures of BAT, and have been extensively used in the study of fatty infiltration in organs such as the heart, liver, pancreas, and skeletal muscles. Thus, the present cross-sectional results are only suggestive of a difference between supraclavicular fossa and subcutaneous depots in infants and children, and the underlying root source of the observed difference in MRI signals can not be uniquely attributed to BAT and WAT.

We recognize several limitations in the present study. First, while the infant cohort had a near equal number of males (n=5) and females (n=7), the children cohort was predominantly males (n=31). This was not intentional and was simply due to the fact that we did not consider gender as a criterion during participant recruitment. Prior literature using PET/CT have reported conflicting observations regarding whether there exists a gender dependence of BAT in pediatric populations (9-11), and it remains an aim for future endeavors to investigate whether the role of BAT in human physiology is mediated differently in males and females. A second limitation was that infants in this study were neural patients at our institution and it is unknown whether their health status or medical condition had any effect on their BAT morphology or metabolic activity prior to their MRI examination. On a related note, anesthesia was not used to sedate infants or children in this study during their MRI exams. It has been recognized that the use of anesthesia can influence the metabolic activity of BAT (24) and hence potentially impact both FF and T_2* measurements. Third, participants in the infant cohort covered only a weight percentile range of 0.8 to 61.9%. Recruitment of additional subjects between the 62% and 100% weight percentile range could have strengthened the present associations between MRI measurements and anthropometry. We were also unable to recruit an adequate number of young children in the age group of 1 to 8 years for this pilot study. The characterization of BAT during this critical growth and developmental period likewise remains an important area for future studies to investigate. Lastly, in the sub-group of children with a BMI percentile greater than 85%, only four subjects were considered overweight (between 85th and 95th BMI percentile). A greater number of subjects in this category would have been beneficial to further compare and contrast against the present 18 subjects that were considered obese (greater than 95th BMI percentile).

We also note several technical limitations related to water-fat MRI in the present study. First, the estimation of T_2* implemented in this work did not explicitly account for the contributions of microscopic and macroscopic B0 field map variations. Both effects can lead

to additional signal dephasing and cause a shorter apparent estimated T_2* value (38, 39). However, we believe that macroscopic susceptibility effects were minimized through the use of small voxels, a high readout bandwidth, and thin slices during data acquisition. We also did not visually notice any sharp and abrupt B0 fieldmap inhomogeneity variations across the supraclavicualar fossa and subcutaneous depots where FF and T_2* measurements were made. Nevertheless, the potential confounding influence of macroscopic susceptibility on apparent tissue T_2* estimation should be considered if B0 field map variation is spatially significant with respect to the acquisition voxel size. We further acknowledge that microscopic susceptibility effects are likely present within BAT adipocytes due to its rich complement of mitochondria organelles laden with iron. However, the proportional contribution of microscopic susceptibility to the apparent T_2* measurements reported in the results were not accounted for in this work.

Another technical limitation is that we adopted only a single T_2* signal model in the present work. This effectively allows one to estimate the apparent tissue T_2* within each imaging voxel, but not individually for water and fat components. While an extended dual T_2* model has been proposed to estimate individually the water and fat component relaxation rates (30), it remains unclear presently whether this extension can elucidate additional signal contrast in BAT characterization. Lastly, we recognize that the present mDIXON work utilized a precalibrated spectral modeling of fat based on human bone marrow and subcutaneous adipose tissue (27), and not directly of BAT. However, it has been shown that the spectral characteristics of triglycerides between BAT and WAT are quite similar, with only subtle differences in chain length and degree of carbon unsaturation (40). Furthermore, several recent literature reports have shown that the estimated FF is minimally impacted by moderate differences in the fat spectral models assumed during water-fat decomposition and image reconstruction (41, 42). The use of an appropriate multi-peak fat spectral model is nonetheless more accurate than the traditional single-peak water-methylene model.

From Table 3, the difference in the presence and absence of correlations observed between FF, T_2*, and anthropometric measurements in infants and children suggests potential differences in BAT physiology between these two age groups that warrant further investigations. Several recent works have suggested evidence and biochemical links between BAT, WAT, and skeletal muscle and bone development (43, 44). Existing MRI methods, in combination with novel strategies such as carbon-13 and phosphorous-31 techniques that can quantify tissue metabolic activity, can facilitate new studies to elucidate BAT associations with body adiposity and muscle tone. They can further assist molecular and pharmacological studies that will potentially lead to promising strategies aimed at facilitating the recruitment of brown adipocytes and the promotion of “brite” adipocyte differentiation (45). Studies are also needed to examine the degree with which BAT accounts for phenotypic differences among healthy infants, its implication in pediatric endocrinology, obesity prevention and treatment, its involvement in growth and development, and the degree to which BAT is influenced by maternal health, gestational age, birth weight, and nutrition.

In conclusion, this work has offered evidence that MRI is capable of characterizing BAT and WAT in vivo, particularly in infants. Presently, PET/CT remains the preferred modality for investigating metabolically active BAT, and findings in adults continue to emerge. There is however a paucity of BAT data in pediatric populations. The intrinsic differences between BAT and WAT adipocytes and the observation that there exists inter-subject variations within the supraclavicular fossa adipose tissue depot which give rise to FF- and T_2*-based MRI signal contrasts, promote a framework for expanding the use of MRI to comparatively study human BAT cross-sectionally in healthy asymptomatic populations, and potentially in

longitudinal studies to assess and monitor changes in BAT characteristics due to stimulation and therapeutic interventions.

Acknowledgments

The authors thank Holger Eggers, Ph.D. from Philips Healthcare for technical support and Lisa Villanueva, Mercedes Landaverde, Nicole Warburton, Arutyun Pogosyan, and Montre Koh for study assistance. The first author (H.H.) is also grateful to for financial support of the James H. Zumberge Award from the Office of the Provost at the University of Southern California.

Funding Support: To VG: National Institutes of Health / NIDDK - R21DK090778

To HH: National Institutes of Health / NIDDK – K25DK087931

To HH: James H. Zumberge Fund, Office of the Provost, University of Southern California

REFERENCES

1. Nedergaard J, Bengtsson T, Cannon B. Three years with adult human brown adipose tissue. Ann N Y Acad Sci. 2010; 1212:E20–36. [PubMed: 21375707]
2. Ravussin E, Galgani JE. The implication of brown adipose tissue for humans. Annu Rev Nutr. 2011; 31:33–47. [PubMed: 21548774]
3. Vijgen GH, Bouvy ND, Teule GJ, Brans B, Schrauwen P, van Marken Lichtenbelt WD. Brown adipose tissue in morbidly obese subjects. PLoS One. 2011; 6:e17247. [PubMed: 21390318]
4. Bartelt A, Bruns OT, Reimer R, et al. Brown adipose tissue activity controls triglyceride clearance. Nat Med. 2011; 17:200–205. [PubMed: 21258337]
5. Yoneshiro T, Aita S, Matsushita M, et al. Age-related decrease in cold-activated brown adipose tissue and accumulation of body fat in healthy humans. Obesity (Silver Spring). 2011; 19:1755–1760. [PubMed: 21566561]
6. Ouellet V, Labbe SM, Blondin DP, et al. Brown adipose tissue oxidative metabolism contributes to energy expenditure during acute cold exposure in humans. J Clin Invest. 2012; 122:545–552. [PubMed: 22269323]
7. Saito M, Okamatsu-Ogura Y, Matsushita M, et al. High incidence of metabolically active brown adipose tissue in healthy adult humans: effects of cold exposure and adiposity. Diabetes. 2009; 58:1526–1531. [PubMed: 19401428]
8. Vijgen GH, Bouvy ND, Teule GJ, et al. Increase in brown adipose tissue activity after weight loss in morbidly obese subjects. J Clin Endocrinol Metab. 2012; 97:E1229–1233. [PubMed: 22535970]
9. Drubach LA, Palmer EL 3rd, Connolly LP, Baker A, Zurakowski D, Cypess AM. Pediatric brown adipose tissue: detection, epidemiology, and differences from adults. J Pediatr. 2011; 159:939–944. [PubMed: 21839465]
10. Gilsanz V, Smith ML, Goodarzian F, Kim M, Wren TA, Hu HH. Changes in brown adipose tissue in boys and girls during childhood and puberty. J Pediatr. 2012; 160:604–609. [PubMed: 22048045]
11. Gilsanz V, Hu HH, Kajimura S. Relevance of brown adipose tissue in infancy and adolescence. Pediatr Res. 2012 doi: 10.1038/pr.2012.141.
12. Lee P, Greenfield JR, Ho KK, Fulham MJ. A critical appraisal of the prevalence and metabolic significance of brown adipose tissue in adult humans. Am J Physiol Endocrinol Metab. 2010; 299:E601–606. [PubMed: 20606075]
13. Lee P, Zhao JT, Swarbrick MM, et al. High prevalence of brown adipose tissue in adult humans. J Clin Endocrinol Metab. 2011; 96:2450–2455. [PubMed: 21613352]
14. Branca RT, Warren WS. In vivo brown adipose tissue detection and characterization using water-lipid intermolecular zero-quantum coherences. Magn Reson Med. 2011; 65:313–319. [PubMed: 20939093]

15. Hu HH, Smith DL Jr. Nayak KS, Goran MI, Nagy TR. Identification of brown adipose tissue in mice with fat-water IDEAL-MRI. J Magn Reson Imaging. 2010; 31:1195–1202. [PubMed: 20432356]
16. Khanna A, Branca RT. Detecting brown adipose tissue activity with BOLD MRI in mice. Magn Reson Med. 2012; 68:1285–1290. [PubMed: 22231619]
17. Chen YI, Cypess AM, Sass CA, et al. Anatomical and functional assessment of brown adipose tissue by magnetic resonance imaging. Obesity (Silver Spring). 2012; 20:1519–1526. [PubMed: 22343821]
18. Hu HH, Hines CD, Smith DL Jr. Reeder SB. Variations in T_2* and fat content of murine brown and white adipose tissues by chemical-shift MRI. Magn Reson Imaging. 2012; 30:323–329. [PubMed: 22244539]
19. Heim T, Hull D. The blood flow and oxygen consumption of brown adipose tissue in the new-born rabbit. J Physiol. 1966; 186:42–55. [PubMed: 5914257]
20. Foster DO, Frydman ML. Nonshivering thermogenesis in the rat. II. Measurements of blood flow with microspheres point to brown adipose tissue as the dominant site of the calorigenesis induced by noradrenaline. Can J Physiol Pharmacol. 1978; 56:110–122. [PubMed: 638848]
21. Sbarbati A, Cavallini I, Marzola P, Nicolato E, Osculati F. Contrast-enhanced MRI of brown adipose tissue after pharmacological stimulation. Magn Reson Med. 2006; 55:715–718. [PubMed: 16506160]
22. Hu HH, Tovar JP, Pavlova Z, Smith ML, Gilsanz V. Unequivocal identification of brown adipose tissue in a human infant. J Magn Reson Imaging. 2012; 35:938–942. [PubMed: 22180228]
23. Eggers H, Brendel B, Duijndam A, Herigault G. Dual-echo Dixon imaging with flexible choice of echo times. Magn Reson Med. 2011; 65:96–107. [PubMed: 20860006]
24. Dicker A, Ohlson KB, Johnson L, Cannon B, Lindahl SG, Nedergaard J. Halothane selectively inhibits nonshivering thermogenesis. Possible implications for thermoregulation during anesthesia of infants. Anesthesiology. 1995; 82:491–501. [PubMed: 7856907]
25. Reeder SB, McKenzie CA, Pineda AR, et al. Water-fat separation with IDEAL gradientecho imaging. J Magn Reson Imaging. 2007; 25:644–652. [PubMed: 17326087]
26. Liu CY, McKenzie CA, Yu H, Brittain JH, Reeder SB. Fat quantification with IDEAL gradient echo imaging: correction of bias from T1 and noise. Magn Reson Med. 2007; 58:354–364. [PubMed: 17654578]
27. Ren J, Dimitrov I, Sherry AD, Malloy CR. Composition of adipose tissue and marrow fat in humans by 1H NMR at 7 Tesla. J Lipid Res. 2008; 49:2055–2062. [PubMed: 18509197]
28. Ghugre NR, Wood JC. Relaxivity-iron calibration in hepatic iron overload: probing underlying biophysical mechanisms using a Monte Carlo model. Magn Reson Med. 2011; 65:837–847. [PubMed: 21337413]
29. Hines CD, Agni R, Roen C, et al. Validation of MRI biomarkers of hepatic steatosis in the presence of iron overload in the ob/ob mouse. J Magn Reson Imaging. 2012; 35:844–851. [PubMed: 22127834]
30. Horng DE, Hernando D, Hines CD, Reeder SB. Comparison of R_2* correction methods for accurate fat quantification in fatty liver. J Magn Reson Imaging. 2012 doi: 10.1002/jmri.23835.
31. Enerback S. Human brown adipose tissue. Cell Metab. 2010; 11:248–252. [PubMed: 20374955]
32. Heaton JM. The distribution of brown adipose tissue in the human. J Anat. 1972; 112:35–39. [PubMed: 5086212]
33. Spalding KL, Arner E, Westermark PO, et al. Dynamics of fat cell turnover in humans. Nature. 2008; 453:783–787. [PubMed: 18454136]
34. Tchoukalova YD, Koutsari C, Karpyak MV, Votruba SB, Wendland E, Jensen MD. Subcutaneous adipocyte size and body fat distribution. Am J Clin Nutr. 2008; 87:56–63. [PubMed: 18175737]
35. Ichimiya H, Arakawa S, Sato T, et al. Involvement of brown adipose tissue in subcutaneous fat necrosis of the newborn. Dermatology. 2011; 223:207–210. [PubMed: 21968020]
36. Symonds ME, Pope M, Sharkey D, Budge H. Adipose tissue and fetal programming. Diabetologia. 2012; 55:1597–1606. [PubMed: 22402988]

37. Silverman WA, Zamelis A, Sinclair JC, Agate FJ. Warm nape of the newborn. Pediatrics. 1964; 33:984–987. [PubMed: 14169648]

38. Weisskoff RM, Zuo CS, Boxerman JL, Rosen BR. Microscopic susceptibility variation and transverse relaxation: theory and experiment. Magn Reson Med. 1994; 31:601–610. [PubMed: 8057812]

39. Hernando D, Vigen KK, Shimakawa A, Reeder SB. R2* mapping in the presence of B0 field variations. Magn Reson Med. 2012; 68:830–840. [PubMed: 22161866]

40. Hamilton G, Smith DL, Bydder M, Nayak KS, Hu HH. Magnetic resonance properties of brown and white adipose tissues. J of Magn Reson Imaging. 2011; 34:468–473. [PubMed: 21780237]

41. Yokoo T, Shiehmorteza M, Hamilton G, et al. Estimation of hepatic fat fraction by using MR imaging at 3.0T. Radiology. 2011; 258:749–759. [PubMed: 21212366]

42. Kühn JP, Hernando D, Muñoz del Rio A, et al. Effect of multipeak spectral modeling of fat for liver iron and fat quantification: correlation of biopsy with MR imaging results. Radiology. 2012; 265:133–142. [PubMed: 22923718]

43. Bostrom P, Wu J, Jedrychowski MP, et al. A PGC1-alpha-dependent myokine that drives brown-fat-like development of white fat and thermogenesis. Nature. 2012; 481:463–468. [PubMed: 22237023]

44. Krings A, Rahman S, Huang S, Lu Y, Czernik PJ, Lecka-Czernik B. Bone marrow fat has brown adipose tissue characteristics, which are attenuated with aging and diabetes. Bone. 2012; 50:546–552. [PubMed: 21723971]

45. Ishibashi J, Seale P. Beige can be slimming. Science. 2010; 328:1113–1114. [PubMed: 20448151]

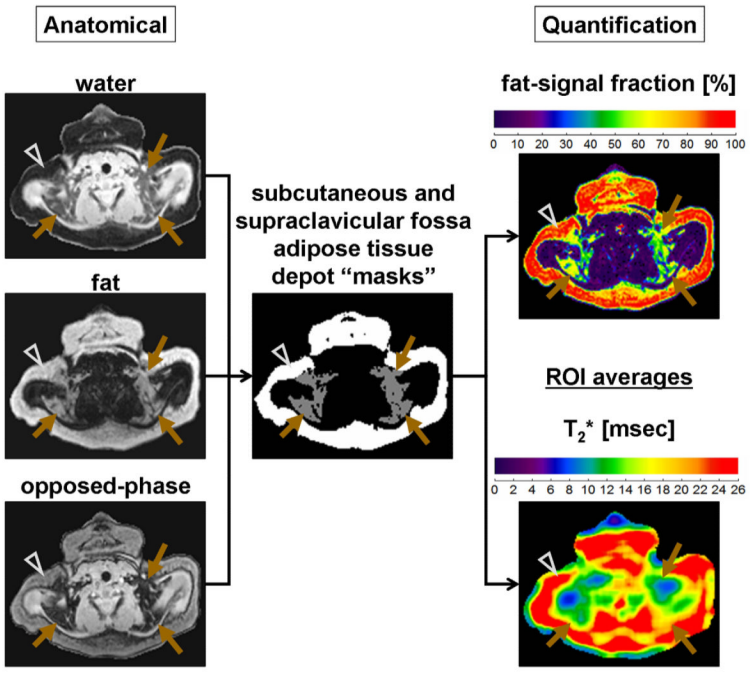

Figure 1.

Anatomical grayscale images of water, fat, and opposed-phase images are used to manually create segmentation masks for the subcutaneous (arrowheads) and supraclavicular (brown arrows) adipose tissue depots. The binary masks are generated using commercial sliceOmatic® software using a combination of signal-intensity based thresholding, region growing, and morphological erosion steps. The generated masks are then automatically transferred by the software to the co-registered FF and T_2* maps, shown in color, to compute region-of-interest (ROI) values. Images are from a 66-days-old boy. The FF maps are illustrated on a 0% (purple) to 100% (red) scale. The T_2* maps are illustrated using a condensed scale from 0 to 26 msec for illustration clarity, such that any tissue with a computed T_2* value ≥ 26 msec is shown in red.

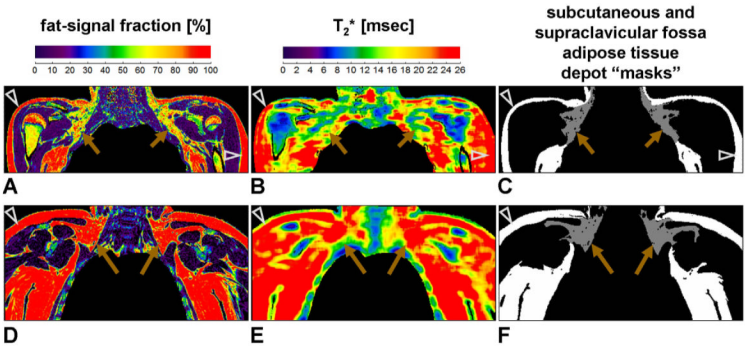

Figure 2.

(A) FF map, **(B)** T_2* map, and **(C)** segmentation masks from a 15-years-old female with a healthy BMI of 22.2 kg/m^2, and **(D-F)** a 12-years-old female with an obese BMI of 31.4 kg/m^2. Note the relatively well-defined supraclavicular fossa depot and the detail with which the segmentation masks are generated by the sliceOmatic® software. Note the exclusion of non-adipose tissue structures. Same arrowhead and arrow symbols, as well as color scale notations, as Figure 1.

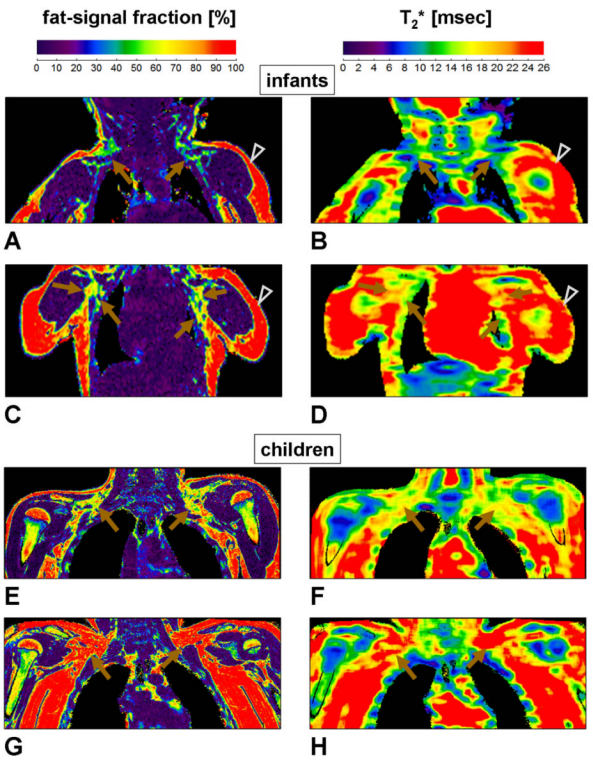

Figure 3.

Representative FF **(left column, A, C, E, G)** and T_2* **(right column, B, D, F, H)** maps from **(A-D)** two infants and **(E-H)** two children. The infant illustrated in **(A, B)** is a 123-days-old girl with a weight percentile of 10%. The infant illustrated in **(C, D)** is a 100-days-old girl with a weight percentile of 25%. Bilateral supraclavicular fossa depots where BAT is typically found are highlighted (brown arrows). Note that these BAT-containing depots are visually distinguishable from the triglyceride-rich (red) subcutaneous white adipose tissue depot (arrowheads) and lean skeletal muscles and organs (purple) in the FF maps. Note that their appearance also differs between the two infants. Corresponding areas on the T_2* maps also show lower values in the supraclavicular fossa depot in comparison to the subcutaneous depot. FOV settings for **(A, B)** were: right/left 24 cm, anterior/posterior 14 cm, and superior/inferior 10 cm. For **(C, D)** they were: right/left 22 cm, anterior/posterior 14 cm, and superior/inferior 10 cm. The child illustrated in **(E, F)** is a lean 12-years-old male with a BMI of 17.2 kg/m^2 and a BMI percentile of 35.3%. The child illustrated in **(G, H)** is an obese 11-years-old male with a BMI of 32.7 kg/m^2 and a BMI percentile of 99.2%. The difference in both FF and T_2* appearances within the supraclavicular fossa BAT depot is markedly evident between the two children, with BAT in the lean subject characterized by lower values. FOV settings for **(E, F)** were: right/left 36 cm, anterior/posterior 16 cm, and superior/inferior 25 cm. For **(G, H)** they were: right/left 44 cm, anterior/posterior 26 cm, and superior/inferior 25 cm. Same arrowhead and arrow symbols, as well as color scale notations, as Figure 1.

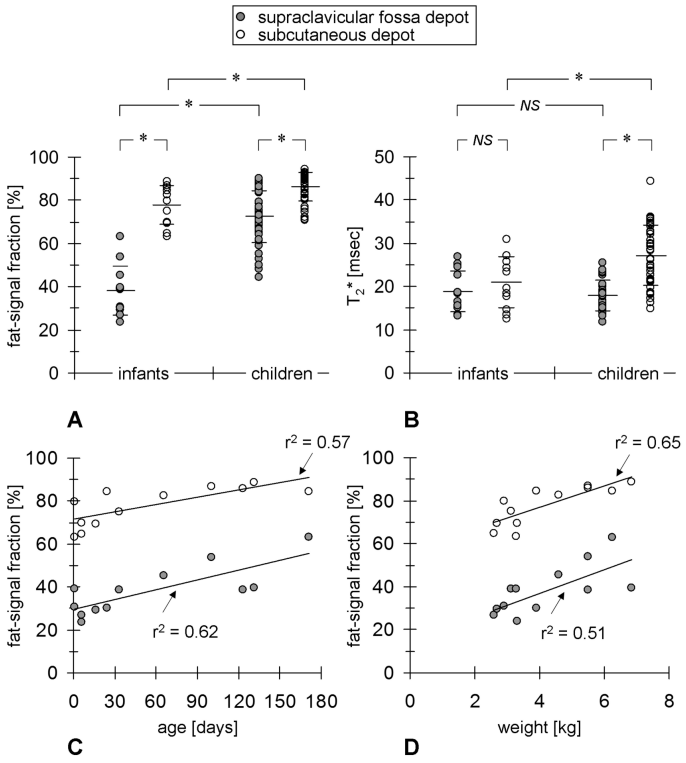

Figure 4.

Comparison of **(A)** FF and **(B)** T_2* distributions between all infants (n=12) and all children (n=39) from the study from measurements within the supraclavicular fossa depot (filled circles) and subcutaneous depot (open circles). The long horizontal bar in each distribution denotes the mean while the pair of short horizontal bars denotes standard deviation. Statistically significant comparisons are denoted by (*) for $p<0.01$. Statistically significant correlations were observed between FF values and infant age **(C)** and weight **(D)** in both depots. See also Table 3.

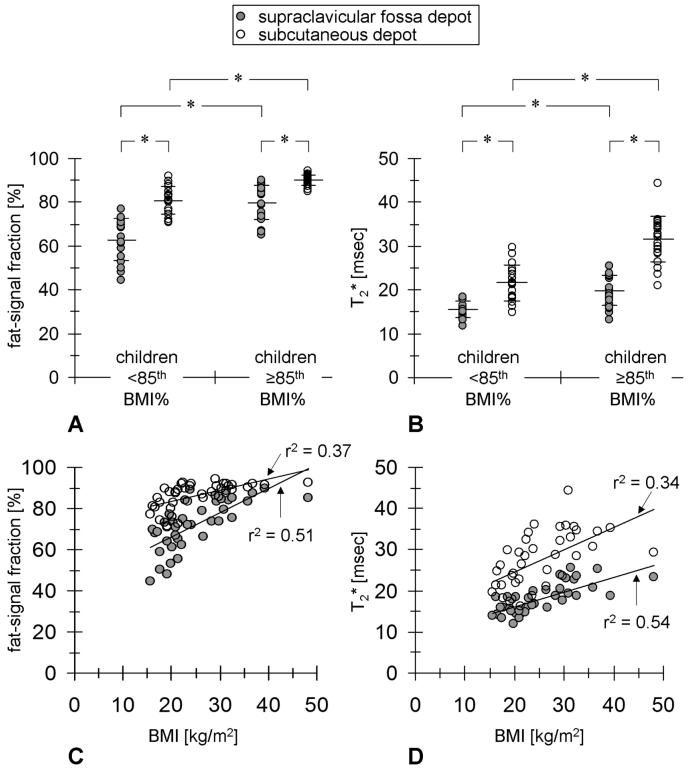

Figure 5.

Comparison of **(A)** FF and **(B)** T_2* distributions between lean (n=17) and overweight/obese (n=22) children sub-groups, stratified at the 85th BMI percentile. Same symbol notation as Figure 4. Statistically significant correlations were observed between **(C)** FF and **(D)** T_2* values versus BMI in both depots. See also Table 3.

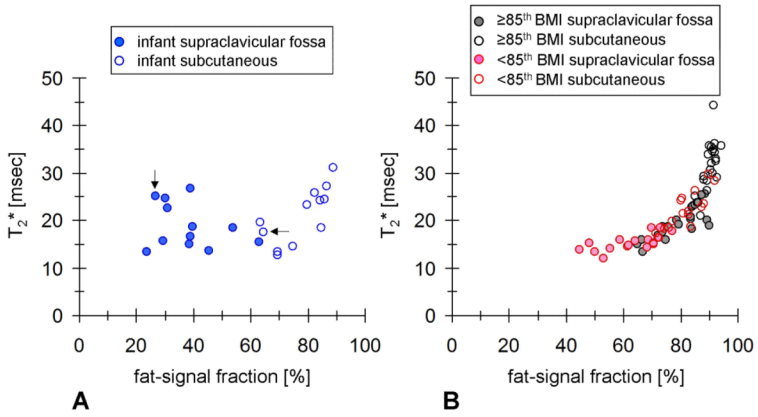

Figure 6.

Scatter plots of individual mean FF and T_2* values for **(A)** the infant cohort and **(B)** the children cohort. Filled circles represent measurements from the supraclavicular fossa depot. Open circles represent measurements from the subcutaneous depot. While there does not appear to be a data trend in the infants, it is clear that FF values in the supraclavicular fossa depot are lower than that of the subcutaneous depot. However, T_2* values are similar. The data trend in the children cohort is in contrast visually striking and suggests associations between FF and T_2* measurements in the two depots with body adiposity. For visual clarity, the two plots were not overlaid on top of each other. However, note that they share the same axes. In **(A)**, the data point pair highlighted by arrows denote the infant illustrated in Figure 7.

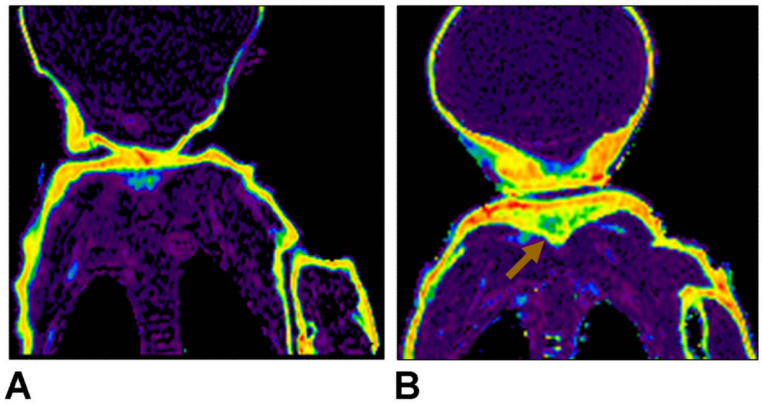

Figure 7.

FF maps from a 6-days-old girl, shown on the same 0-100% scale as in Figures 1-3. In **(A)** note the rather low (yellow-orange) FF appearance of the subcutaneous depot (~64.6%), suggestive of potential BAT presence. In **(B)**, the triangular adipose tissue depot located at the nape is evident (arrow), with an FF appearance also supportive of BAT presence.

Table 1

Summary of anthropometric and MRI measurements for the infant cohort (n=12, 5 males, 7 females). Note that age is reported in days.

	Mean (SD) Range
Age [days]	56.5 (60.0) 1.0 – 171.0
Weight [kg]	4.2 (1.5) 2.6 – 6.8
Weight Percentile	22.3 (21.5) 0.8 – 61.9
BAT FF [%]	38.2 (11.5) 23.8 – 63.1
BAT T_2* [msec]	18.8 (4.8) 13.3 – 26.8
WAT FF [%]	77.9 (9.1) 63.2 – 88.9
WAT T_2* [msec]	21.0 (5.9) 12.6 – 31.0

SD: standard deviation

BAT: brown adipose tissue

WAT: white adipose tissue

FF: fat-signal fraction

Table 2

Summary of anthropometric and MRI measurements for the children cohort (n=39, 31 males, 8 females). P-values are provided for comparisons between the two BMI percentile groups (Lean vs. Overweight/Obese).

	Mean (SD) Range			
	All (n=39)	**Lean BMI percentile < 85% (n=17)**	**Overweight / Obese BMI percentile ≥ 85% (n=22)**	**p-value**
Age [years]	13.4 (2.8) 9.2 – 19.0	14.3 (2.7) 9.2 – 18.8	12.7 (2.7) 9.2 – 19.0	0.08
Weight [kg]	63.5 (23.4) 30.2 – 128.2	49.2 (12.2) 30.0 – 67.9	74.5 (24.3) 39.0 – 128.2	<0.01
Weight Percentile	73.7 (29.8) 0.0 – 99.9	45.8 (24.4) 0.0 – 78.9	95.3 (6.0) 76.3 – 99.9	<0.01
BMI [kg/m^2]	25.1 (7.3) 15.6 – 48.2	19.2 (2.2) 15.6 – 23.5	29.8 (6.5) 21.0 – 48.2	<0.01
BMI Percentile	74.7 (31.0) 4.0 – 99.7	45.6 (26.0) 4.0 – 83.6	97.2 (2.4) 91.3 – 99.7	<0.01
BAT FF [%]	72.5 (12.1) 44.5 – 89.9	62.9 (9.9) 44.5 – 77.0	79.9 (7.7) 65.1 – 89.9	<0.01
BAT T_2* [msec]	18.0 (3.6) 11.9 – 25.5	15.5 (1.9) 11.9 – 18.5	19.9 (3.4) 13.3 – 25.5	<0.01
WAT FF [%]	86.2 (6.5) 70.7 – 94.2	80.9 (6.5) 70.7 – 91.9	90.3 (2.3) 85.0 – 94.2	<0.01
WAT T_2* [msec]	27.2 (6.8) 15.0 – 44.4	21.6 (4.1) 15.0 – 29.7	31.6 (5.1) 21.0 – 44.4	<0.01

SD: standard deviation

BMI: body-mass-index

BAT: brown adipose tissue

WAT: white adipose tissue

FF: fat-signal fraction

Table 3

Summary of statistically significant linear regression correlation coefficients between anthropometric variables and MRI measurements.

	correlation coefficient (r) for supraclavicular fossa BAT				correlation coefficient (r) fors ubcutaneous WAT			
	All Infants (n=12)		All Children (n=39)		All Infants (n=12)		All Children (n=39)	
	FF	T_2*	FF	T_2*	FF	T_2*	FF	T_2*
Age	0.79 [a, *]	-	-	-	0.76 [a, *]	-	-	-
Weight [kg]	0.71 [a, *]	-	0.54 [*]	0.50 [*]	0.81 [a, *]	0.67 [+]	0.35 [*]	0.32
Weight Percentile	-	-	0.59 [*]	0.54 [*]	-	-	0.59 [*]	0.60 [*]
BMI [kg/m^2]	-	-	0.71 [b, *]	0.74 [b, *]	0.59 [+]	-	0.61 [b, *]	0.59 [b, *]
BMI Percentile	-	-	0.65 [*]	0.57 [*]	-	-	0.70 [*]	0.66 [*]

BMI: body-mass-index

BAT: brown adipose tissue

WAT: white adipose tissue

FF: fat-signal fraction

[a] See Figure 4C and 4D

[b] See Figure 5C and 5D

[*] Statistically significant ($p<0.01$)

[+] Statistically significant ($p<0.05$)

[-] Not statistically significant